



Silver-inserted heterojunction photocatalyst consisting of zinc rhodium oxide and silver antimony oxide for overall pure-water splitting under visible light



Yoshiki Hara ^a, Toshihiro Takashima ^{a,b,c}, Ryoya Kobayashi ^b, Sameera Abeyrathna ^b, Bunsho Ohtani ^d, Hiroshi Irie ^{a,b,c,e,*}

^a School of Engineering, University of Yamanashi, 4-3-11 Takeda, Kofu, Yamanashi 400-8511, Japan

^b Special Doctoral Program for Green Energy Conversion Science and Technology, Interdisciplinary Graduate School of Medicine and Engineering, University of Yamanashi, 4-3-11 Takeda, Kofu, Yamanashi 400-8511, Japan

^c Clean Energy Research Center, University of Yamanashi, 4-3-11 Takeda, Kofu, Yamanashi 400-8511, Japan

^d Institute for Catalysis, Hokkaido University, Nishi 10, Kita 21, Sapporo 001-0021, Japan

^e Cooperative Research Fellow, Institute for Catalysis, Hokkaido University, Nishi 10, Kita 21, Sapporo 001-0021, Japan

ARTICLE INFO

Article history:

Received 16 February 2017

Received in revised form 7 March 2017

Accepted 15 March 2017

Available online 18 March 2017

Keywords:

Two-step overall water-splitting

Zinc rhodium oxide

Silver antimony oxide

Silver

Ammonia treatment

ABSTRACT

Overall pure-water splitting under visible-light irradiation at wavelengths up to 660 nm was accomplished utilizing a solid-state hetero-junction photocatalyst following the Z-scheme mechanism in which zinc rhodium oxide ($ZnRh_2O_4$) and silver antimony oxide ($AgSbO_3$) as hydrogen (H_2)- and oxygen (O_2)-evolution photocatalysts, respectively, were connected with silver (Ag , $ZnRh_2O_4/Ag/AgSbO_3$). In our previous paper (Kobayashi et al., *J. Phys. Chem. C*, 118 (2014) 22450–22456), nitric acid (HNO_3) treatment of mixtures of $AgSbO_3$, Ag_2O , and $ZnRh_2O_4$ after calcination formed defective $AgSbO_3$ ($Ag_{1-x}SbO_3-y$) and the resulting photocatalyst, $ZnRh_2O_4/Ag/Ag_{1-x}SbO_3-y$, exhibited reduced visible-light wavelength sensitivity (up to 545 nm) and overall water-splitting activity. To overcome this limitation, here, unnecessary Ag was removed by treatment with ammonium hydroxide (NH_4OH) and hydrogen peroxide (H_2O_2), which resulted in the successful formation of $ZnRh_2O_4/Ag/AgSbO_3$. This photocatalyst was capable of utilizing visible light at wavelengths up to 660 nm and exhibited enhanced overall water-splitting activity. The synthesis approach described in this study represents a novel and facile method for preparing visible-light sensitive heterojunction photocatalysts connected with Ag .

© 2017 Elsevier B.V. All rights reserved.

1. Introduction

Various photocatalytic materials have been evaluated for solar-based hydrogen production by water splitting because the generated hydrogen (H_2) represents a clean and renewable fuel source [1]. In addition, water splitting using a powdered photocatalyst is a relatively simple reaction that is potentially scalable [2,3]. To date, most research has focused on increasing the sensitization of catalysts to visible light to allow the more efficient utilization of solar energy [5–20]. Several photocatalysts, including gallium nitride (GaN)-zinc oxide (ZnO) solid-solution [4], zinc-germanium oxynitride ($(Zn_{1.44}Ge)(N_2O_{0.44})$) [5], bismuth-yttrium-tungsten ternary oxide ($BiYW_6$) [6], and niobium-substituted silver-

tantalum oxide ($AgTa_{0.7}Nb_{0.3}O_3$), are able to split pure water into H_2 and O_2 in stoichiometric amounts in the presence of an appropriate cocatalyst [7]. Recently, nano-particulate CoO with a band-gap of 2.6 eV was reported to split pure water under visible-light irradiation without the requirement for a co-catalyst [8]. A complex photocatalyst consisting of titanium and silicon amorphous oxyhydroxide ($MO_{2-m}(OH)_{2m-x}H_2O$)-coated Rh - Cr oxide ($RhCrO_y$)-loaded lanthanum-magnesium-tantalum oxynitride ($LaMg_xTa_{1-x}O_{1+3x}N_{2-3x}$) was also shown to have photocatalytic water-splitting activity at wavelengths up to 600 nm [9]. In addition, Liu et al. [10] reported that a carbon nanodot-carbon nitride (C_3N_4) nanocomposite was capable of overall water splitting under irradiation at a wavelength of 630 ± 20 nm.

A number of H_2 evolution (H_2 -photocatalysts) and O_2 evolution photocatalysts (O_2 -photocatalysts) generate either H_2 or O_2 (half reaction of water), respectively, when irradiated with visible light the presence of a sacrificial agent [11–16]. Combinations of

* Corresponding author at: Clean Energy Research Center, University of Yamanashi, 4-3-11 Takeda, Kofu, Yamanashi 400-8511, Japan.

E-mail address: hirie@yamanashi.ac.jp (H. Irie).

these photocatalysts, such as platinum (Pt)-deposited chromium and tantalum-codoped strontium titanate (Pt/SrTiO₃:Cr,Ta), and rhodium (Rh)-doped SrTiO₃ (SrTiO₃:Rh) as the H₂-photocatalyst, and Pt-deposited WO₃ or bismuth vanadate (BiVO₄) as the O₂-photocatalyst, are capable of overall water-splitting under visible-light irradiation [17–19]. However, because such two-step photoexcitation systems, which are termed “Z-scheme”, require a suitable redox mediator, such as iodate ion (IO₃[−])/iodide ion (I[−]) or ferric ion (Fe³⁺)/ferrous ion (Fe²⁺), these systems cannot split water using “pure” water (i.e., distilled water without chemicals). Recently, two solid-state Z-scheme systems, ruthenium (Ru)-loaded SrTiO₃:Rh (Ru/SrTiO₃:Rh) and BiVO₄ with and without photoreduced graphene oxide (PRGO; PRGO/BiVO₄ and BiVO₄, respectively), were shown to function as overall water-splitting photocatalysts in the absence of a redox mediator under visible-light irradiation [20,21]. Notably, however, because the photoactivity of Ru/SrTiO₃:Rh, BiVO₄, and PRGO/BiVO₄ is dependent on the formation of aggregates, which require acidic conditions (pH 3.5, adjusted with H₂SO₄) to generate attractive electrostatic surface interactions, these compounds are not considered to be capable of splitting water using pure water.

We developed two novel solid-state photocatalysts by inserting silver (Ag) as an electron mediator between zinc rhodium oxide (ZnRh₂O₄, E_g of 1.2 eV) as the H₂-photocatalyst and defective silver antimonate (Ag_{1-x}SbO_{3-y}, E_g of 2.7 eV) or bismuth vanadate (Bi₄V₂O₁₁; E_g of 1.7 eV) as the O₂-photocatalyst (ZnRh₂O₄/Ag/Ag_{1-x}SbO_{3-y} [22] and ZnRh₂O₄/Ag/Bi₄V₂O₁₁ [23,24], respectively). In these systems, the overall water-splitting of pure water proceeded via Ag, which mediated the transfer of photoexcited electrons from the conduction band (CB) of the O₂-photocatalyst to the valence band (VB) of the H₂-photocatalyst. ZnRh₂O₄/Ag/Ag_{1-x}SbO_{3-y} and ZnRh₂O₄/Ag/Bi₄V₂O₁₁ were capable of utilizing visible light at wavelengths of 545 and 740 nm, respectively, a property that was determined by the photoactivity of Ag_{1-x}SbO_{3-y} and Bi₄V₂O₁₁. To achieve overall pure-water splitting by these materials, treatment with nitric acid (HNO₃) is required to remove excess Ag, which acts as a sacrificial agent for O₂ evolution. However, HNO₃ treatment leads to the formation of Ag_{1-x}SbO_{3-y}, which results in the decreased activity, and bandgap expansion leading to a reduction in the utilizable wavelength region, thereby decreasing overall water-splitting reaction. HNO₃ treatment causes a similar reduction in the photoactivity of Bi₄V₂O₁₁, as this O₂-photocatalyst partially dissolves in aqueous HNO₃.

In an attempt to develop a solid-state photocatalyst with improved visible-light sensitivity and water-splitting activity, here, ZnRh₂O₄/Ag/AgSbO₃ was prepared by the treatment with ammonium hydroxide (NH₄OH) and hydrogen peroxide (H₂O₂) to remove excess Ag in place of HNO₃. Using this approach, the wavelength region of utilizable visible light was increased to 660 nm and the overall water-splitting activity of ZnRh₂O₄/Ag/AgSbO₃ was enhanced.

2. Experimental section

2.1. Sample preparation

ZnRh₂O₄ and AgSbO₃ powders were synthesized using a conventional solid-state reaction method. Briefly, commercial zinc oxide (ZnO, purity 99.0%; Kanto Kagaku) and rhodium oxide (Rh₂O₃, purity 99.9%; Kanto Kagaku) powders were used as starting materials for the synthesis of ZnRh₂O₄, and silver oxide (Ag₂O, purity 99.0%; Kanto Kagaku) and antimony oxide (Sb₂O₅, purity 99.995%; Sigma-Aldrich) powders were used as starting materials for the synthesis of AgSbO₃. Stoichiometric amounts of the starting materials for each photocatalyst were wet ball milled for 20 h

using zirconium dioxide (ZrO₂) balls as the milling medium. The resulting mixtures were calcined in air atmosphere at 1000 °C for 24 h to generate ZnRh₂O₄ and at 900 °C for 8 h to generate AgSbO₃. The obtained powders were thoroughly ground with a mortar and pestle.

ZnRh₂O₄–Ag–AgSbO₃ hetero-junction photocatalyst (ZnRh₂O₄/Ag/AgSbO₃) powder was prepared as follows. AgSbO₃, Ag₂O, and ZnRh₂O₄ (molar ratio of 0.8:1.0:1.2) were wet ball milled as described above. The mixed powders were pressed at 60-kN force to form pellets, which were then heated at 900 °C for 2 h. After grinding the pellets into fine powder with a mortar and pestle, 150 mg of the powder was suspended in 300 mL ammonia solution (NH₄OH, 5 mol L^{−1}) with a pH adjusted to 9.8 using concentrated (13 mol L^{−1}) nitric acid (HNO₃). The resulting suspension was mixed with 300 μL hydrogen peroxide (H₂O₂, 8.8 mol L^{−1}). After stirring for 6.5 min the resultant powder was recovered by filtration, washed with a sufficient amount of distilled water, and then dried at 65 °C for 3 h. The reaction for the removal of Ag can be expressed as follows: 2Ag + 4NH₄OH + H₂O₂ → 2[Ag(NH₃)₂]⁺ + 2OH[−] + 4H₂O.

2.2. Characterizations

The crystal structures of the prepared powders were determined by X-ray diffraction (XRD) using a PW-1700 instrument (PANalytical). UV–vis absorption (UV–vis) spectra were obtained by the diffuse reflection method using a spectrometer (V-650, Jasco) with barium sulfate (BaSO₄) as the reflectance standard. A scanning electron microscope (SEM, JSM-6500F, JEOL Ltd.) was used to observe the morphology of the prepared photocatalysts. A scanning transmission electron microscope (STEM, Tecnai Osiris, FEI) was also utilized with element maps obtained by energy-dispersive X-ray spectrometry (EDS).

2.3. Photocatalytic water-splitting tests

Photocatalytic overall water-splitting tests were conducted in a gas-closed circulation system. ZnRh₂O₄/Ag/AgSbO₃ composite powder (60 mg) was suspended in 12 mL pure water (pH unadjusted) under an argon atmosphere (50 kPa) and constant stirring using a magnetic stirrer. Light-emitting diode (LED) lamps with wavelengths of 545, 610, 660, and 710 nm (LEDH60-545, −610, −660, and −710 with full widths at half maximum (FWHMs) of 80, 45, 50, 50 nm, respectively, Hamamatsu Photonics) were used for light irradiation. The amounts of evolved H₂ and O₂ were monitored using an online gas chromatograph (GC-8A, Shimadzu). The apparent quantum efficiency (AQE) values were calculated using the amount of evolved O₂ and the equation: AQE (%) = 100 × 4 × O₂ evolution rate/incident photon rate, because O₂ evolution in this system is represented by the formula: 2H₂O + 4h⁺ → O₂ + 4H⁺.

3. Results and discussion

3.1. Characterization

XRD patterns of the prepared photocatalyst powders before and after treatment with NH₄OH and H₂O₂ (hereafter NH₄OH + H₂O₂) are shown in Fig. 1a and b. The XRD patterns of the photocatalyst powders after HNO₃ treatment were also measured as a comparison. The XRD peaks in the spectrum of the untreated powder were attributed to the three phases of ZnRh₂O₄, Ag, and AgSbO₃ (pyrochlore). This assignment is supported by the fact that Ag₂O decomposes to Ag at 280 °C. After treatment of the powder with HNO₃, the peaks corresponding to Ag disappeared, whereas the peaks attributable to ZnRh₂O₄ remain unchanged and those corresponding to AgSbO₃ shifted to a lower 2θ angle. The observed

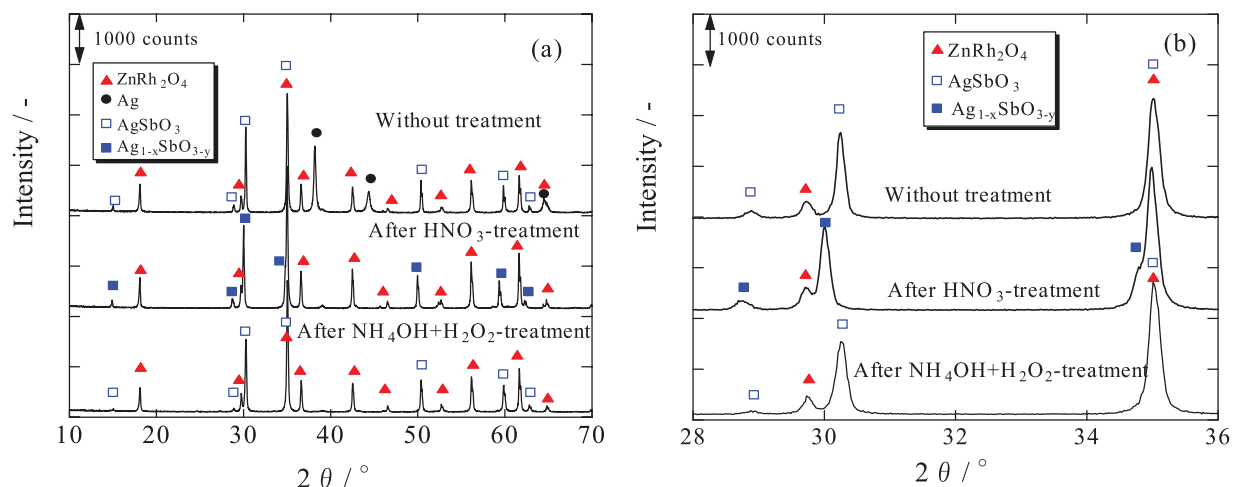


Fig. 1. XRD patterns of $\text{ZnRh}_2\text{O}_4/\text{Ag}/\text{AgSbO}_3$ without treatment, after treatment with HNO_3 , and after treatment with $\text{NH}_4\text{OH} + \text{H}_2\text{O}_2$ (a). (b) is the enlargement of (a).

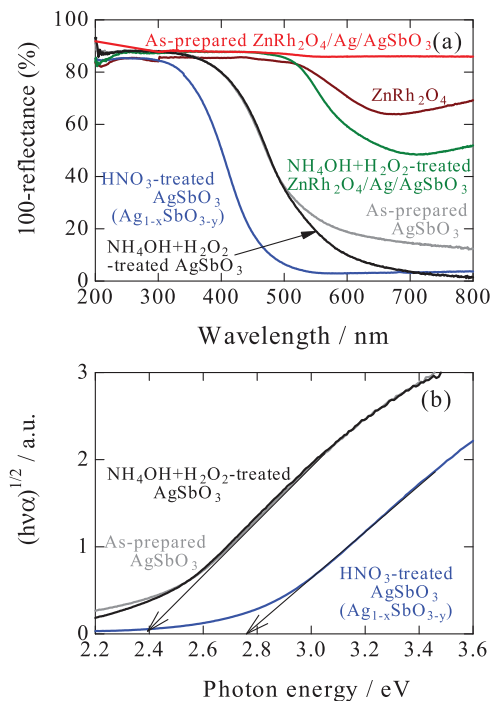


Fig. 2. UV-vis absorption spectra of as-prepared AgSbO_3 , $\text{NH}_4\text{OH} + \text{H}_2\text{O}_2$ -treated AgSbO_3 , HNO_3 -treated AgSbO_3 ($\text{Ag}_{1-x}\text{SbO}_{3-y}$), ZnRh_2O_4 , $\text{ZnRh}_2\text{O}_4/\text{Ag}/\text{AgSbO}_3$ before and after $\text{NH}_4\text{OH} + \text{H}_2\text{O}_2$ treatment (a). Plots of the square root of the Kubelka-Munk functions against photon energy (b). The ends of the two arrows indicate the band-gap energies of as-prepared AgSbO_3 , $\text{NH}_4\text{OH} + \text{H}_2\text{O}_2$ -treated AgSbO_3 , and HNO_3 -treated AgSbO_3 ($\text{Ag}_{1-x}\text{SbO}_{3-y}$) (b).

changes in the XRD patterns indicate that Ag defects were generated in AgSbO_3 as a result of HNO_3 treatment, resulting in the formation of $\text{Ag}_{1-x}\text{SbO}_{3-y}$ ($\text{ZnRh}_2\text{O}_4/\text{Ag}/\text{Ag}_{1-x}\text{SbO}_{3-y}$) [22]. After $\text{NH}_4\text{OH} + \text{H}_2\text{O}_2$ treatment, the peaks corresponding to Ag also disappeared from the XRD spectrum; however, the peaks attributed to AgSbO_3 and ZnRh_2O_4 were unchanged, indicating that both photocatalysts were not modified by the $\text{NH}_4\text{OH} + \text{H}_2\text{O}_2$ treatment.

ZnRh_2O_4 , as-prepared AgSbO_3 , $\text{NH}_4\text{OH} + \text{H}_2\text{O}_2$ -treated AgSbO_3 , HNO_3 -treated AgSbO_3 , and $\text{ZnRh}_2\text{O}_4/\text{Ag}/\text{AgSbO}_3$ before and after $\text{NH}_4\text{OH} + \text{H}_2\text{O}_2$ treatment were analyzed by UV-vis spectrometry (Fig. 2a). The absorption of as-prepared AgSbO_3 above ~ 550 nm was higher than that of $\text{NH}_4\text{OH} + \text{H}_2\text{O}_2$ -treated AgSbO_3 . This finding is

reasonable because the surface of AgSbO_3 particles prepared by the solid-state reaction method contains metallic Ag [25]. Although the metallic Ag was removed by $\text{NH}_4\text{OH} + \text{H}_2\text{O}_2$ treatment (Fig. 1a), as-prepared AgSbO_3 and $\text{NH}_4\text{OH} + \text{H}_2\text{O}_2$ -treated AgSbO_3 had similar absorption edges. In contrast, the absorption edge of HNO_3 -treated AgSbO_3 ($\text{Ag}_{1-x}\text{SbO}_{3-y}$) was shifted to a shorter wavelength region compared to those of as-prepared AgSbO_3 and $\text{NH}_4\text{OH} + \text{H}_2\text{O}_2$ -treated AgSbO_3 .

As AgSbO_3 is an indirect gap semiconductor [26–28], the band-gaps of as-prepared AgSbO_3 , $\text{NH}_4\text{OH} + \text{H}_2\text{O}_2$ -treated AgSbO_3 , and HNO_3 -treated AgSbO_3 ($\text{Ag}_{1-x}\text{SbO}_{3-y}$) were estimated from the x-intercept of tangent lines in plots of the square root of the Kubelka-Munk function against photon energy (Fig. 2b). From the tangent lines, which were extrapolated to $(h\nu\alpha)^{1/2} = 0$, the band-gap of $\text{Ag}_{1-x}\text{SbO}_{3-y}$ was estimated to be 2.7 eV, which was larger than those of HNO_3 - and $\text{NH}_4\text{OH} + \text{H}_2\text{O}_2$ -treated AgSbO_3 (2.4 eV). The observed absorption edge shift of $\text{Ag}_{1-x}\text{SbO}_{3-y}$ was attributable to the formation of Ag defects and a resulting positive shift in the VB top, which is formed from the $4d$ orbitals of Ag. Notably, the absorption of $\text{ZnRh}_2\text{O}_4/\text{Ag}/\text{AgSbO}_3$ following $\text{NH}_4\text{OH} + \text{H}_2\text{O}_2$ treatment decreased from wavelengths longer than ~ 550 nm to an absorption range between that of ZnRh_2O_4 and AgSbO_3 . The decrease in the absorption indicates that Ag was removed from the system.

SEM image analysis of $\text{ZnRh}_2\text{O}_4/\text{Ag}/\text{AgSbO}_3$ powder after $\text{NH}_4\text{OH} + \text{H}_2\text{O}_2$ treatment (hereafter, $\text{ZnRh}_2\text{O}_4/\text{Ag}/\text{AgSbO}_3$) revealed the presence of small ZnRh_2O_4 (~ 200 – 300 nm) and large AgSbO_3 (~ 1000 nm) particles (Fig. 3). STEM imaging and EDS-based elemental mapping of $\text{ZnRh}_2\text{O}_4/\text{Ag}/\text{AgSbO}_3$ were also performed (Fig. 4 and Fig. S1). The large particle in the lower region of the image and the small particles in the upper region correspond to AgSbO_3 and ZnRh_2O_4 , respectively (Fig. 4a). Notably, the AgSbO_3 and ZnRh_2O_4 particles appeared to be connected to each other. Fig. 4b and c show the atomic percentages of Zn, Rh, Ag and Sb measured from the region of ZnRh_2O_4 (A_1) to that of AgSbO_3 (A_2) and in the area of only AgSbO_3 (B_1 – B_2), respectively. In the area corresponding to ZnRh_2O_4 , the atomic percentage of Rh was approximately two-fold higher than that of Zn at a distance of up to ~ 60 nm from A_1 , a result that is consistent with atomic composition of ZnRh_2O_4 particles (Fig. 4b). In the region corresponding to AgSbO_3 (above ~ 100 nm in Fig. 4b and the entire range in Fig. 4c), the atomic percentage of Ag was similar to that of Sb. In contrast, at the interface between ZnRh_2O_4 and AgSbO_3 (~ 60 – 100 nm; Fig. 4b), the percentage of Ag was larger than that of Sb. Taken together, these findings demonstrate

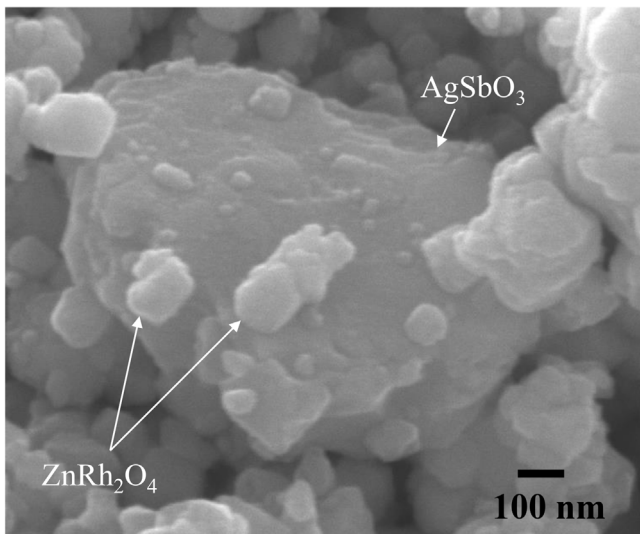


Fig. 3. SEM image of $\text{ZnRh}_2\text{O}_4/\text{Ag}/\text{AgSbO}_3$ after NH_4OH and H_2O_2 treatment.

that Ag was present at the interface of ZnRh_2O_4 and AgSbO_3 and served to bind the two photocatalysts (Fig. S2).

3.2. Photocatalytic water-splitting tests

The time courses of H_2 and O_2 evolution by $\text{ZnRh}_2\text{O}_4/\text{Ag}/\text{AgSbO}_3$ in pure water under irradiation with monochromatic LED lights (545, 610, 660, and 700 nm) were examined to evaluate the AQE values (Fig. 5a–d, respectively). The plots generated by irradiation with 545- and 610-nm LED lights (Fig. 5a and b, solid and open circles, respectively) were used to confirm the reproducibility of the data using the newly prepared $\text{ZnRh}_2\text{O}_4/\text{Ag}/\text{AgSbO}_3$ sample under identical conditions. Although differences in the H_2 and O_2 evolution rates were observed between the prepared samples, H_2 and O_2 were generated at a molar ratio of 2:1 by all samples. H_2 and O_2 evolution at a molar ratio of 2:1 was also observed under 660-nm LED irradiation (Fig. 5c), demonstrating that overall pure-water

splitting was accomplished at this wavelength. In contrast, under irradiation with 700-nm LED, H_2 and O_2 appeared to be generated simultaneously; however, the ratio of H_2 and O_2 was not 2:1 (Fig. 5d), indicating that the overall pure-water splitting reaction did not proceed.

We next calculated the total number of incident photons from each LED light source and the O_2 -evolution rates from the slopes of the plots in Fig. 5a–c, and used these values to estimate the AQE for each condition (Fig. 6, black solid circles, and Table S1). For 700-nm LED light, the AQE value was considered to be zero, as overall pure-water splitting by the $\text{ZnRh}_2\text{O}_4/\text{Ag}/\text{AgSbO}_3$ sample did not proceed. The obtained AQE values for O_2 evolution were almost identical to those for H_2 evolution because the H_2 and O_2 evolution rates were 2:1. In addition, it was determined that the AQE values coincided with the UV-vis spectra of $\text{NH}_4\text{OH} + \text{H}_2\text{O}_2$ -treated AgSbO_3 , but did not match that of as-prepared AgSbO_3 , which contains metallic silver, nor that of HNO_3 -treated AgSbO_3 , which is defective for $\text{Ag}(\text{Ag}_{1-x}\text{SbO}_{3-y})$ (Fig. 6). This finding indicates that the overall pure-water splitting over $\text{ZnRh}_2\text{O}_4/\text{Ag}/\text{AgSbO}_3$ proceeded at wavelengths up to 660 nm via excitation of AgSbO_3 , as well as ZnRh_2O_4 , which has a band-gap of 1.2 eV and can therefore absorb light of longer wavelengths than AgSbO_3 . The AQE values therefore reflected the photoabsorption capacity of AgSbO_3 . $\text{ZnRh}_2\text{O}_4/\text{Ag}/\text{AgSbO}_3$ can split water under irradiation with visible light up to 660 nm longer than the wavelength corresponding to the band-gap energy of AgSbO_3 . This photosensitivity to longer wavelength would be caused by the tailing of its absorption spectrum (Fig. 2a), presumably caused by Ag 4d orbitals forming the VB top of AgSbO_3 . The AQE values for $\text{ZnRh}_2\text{O}_4/\text{Ag}/\text{Ag}_{1-x}\text{SbO}_{3-y}$ were reported in our previous paper (0.010% and 0.012% at 505 nm, 0.0012% at 545 nm, and 0% at 610 nm) [22] and are presented here in Fig. 6 (blue solid circles). $\text{ZnRh}_2\text{O}_4/\text{Ag}/\text{Ag}_{1-x}\text{SbO}_{3-y}$, which was generated by HNO_3 treatment to remove excess Ag, utilizes wavelengths of up to 545 nm due to the wide band-gap of $\text{Ag}_{1-x}\text{SbO}_{3-y}$, which determines the photo-availability of the system. At 545 nm, the AQE for $\text{ZnRh}_2\text{O}_4/\text{Ag}/\text{AgSbO}_3$ was over 100-fold larger than that for $\text{ZnRh}_2\text{O}_4/\text{Ag}/\text{Ag}_{1-x}\text{SbO}_{3-y}$. Thus, by treating mixtures of AgSbO_3 , Ag_2O , and ZnRh_2O_4 after calcination with $\text{NH}_4\text{OH} + \text{H}_2\text{O}_2$ in place of HNO_3 to generate $\text{ZnRh}_2\text{O}_4/\text{Ag}/\text{AgSbO}_3$ rather than $\text{ZnRh}_2\text{O}_4/\text{Ag}/\text{Ag}_{1-x}\text{SbO}_{3-y}$, the wavelength of utilizable visible light

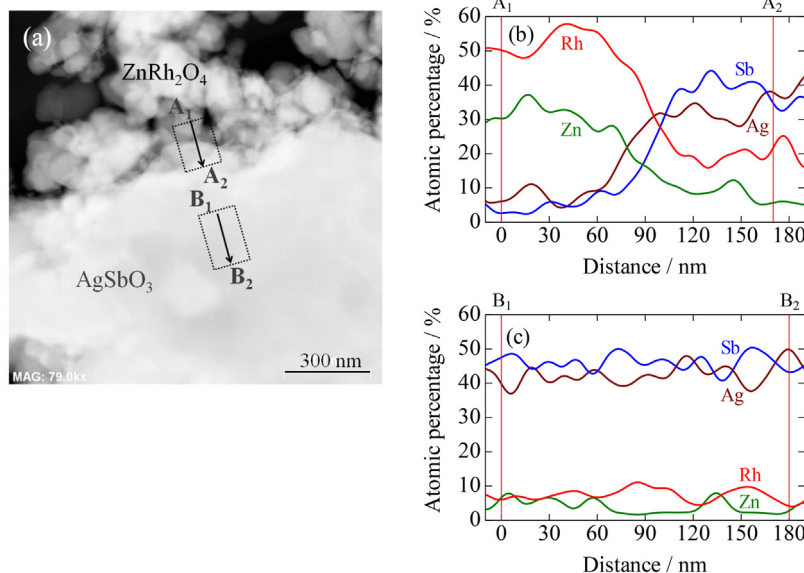


Fig. 4. STEM image of $\text{ZnRh}_2\text{O}_4/\text{Ag}/\text{AgSbO}_3$ (a). In (a), the rectangles denoted by broken lines represent the areas subjected to elemental analyses for Zn, Rh, Ag, and Sb, and the analysis centers and directions (from A_1 to A_2 and B_1 to B_2) are indicated by arrows. The atomic percentages of Zn, Rh, Ag, and Sb measured from the area of ZnRh_2O_4 (A_1) to that of $\text{Ag}_{1-x}\text{SbO}_{3-y}$ (A_2) (b) and in the area of only AgSbO_3 (B_1 to B_2) are shown (c).

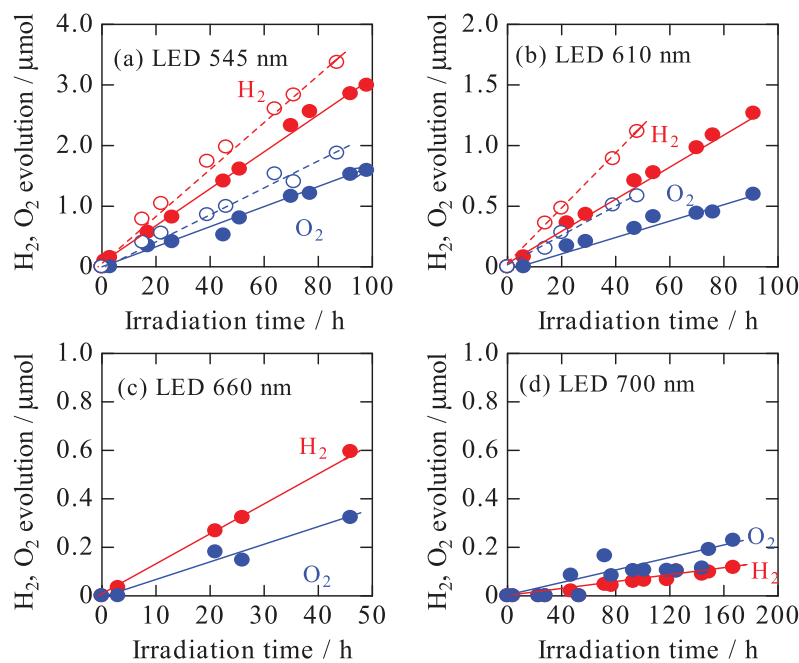


Fig. 5. Time courses of the photocatalytic evolution of H_2 and O_2 from pure water in the presence of $\text{ZnRh}_2\text{O}_4/\text{Ag}/\text{AgSbO}_3$ under irradiation with LED light at 545 nm (a), 610 nm (b), 660 nm (c), and 700 nm (d).

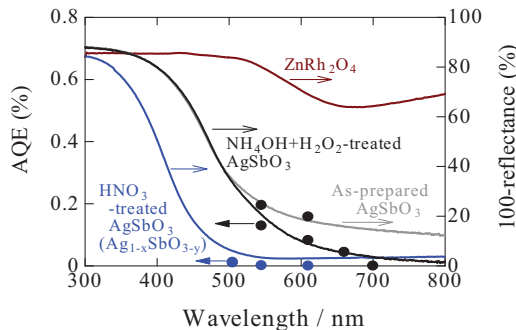


Fig. 6. Apparent quantum efficiencies (AQE) for photocatalytic O_2 evolution from pure water by $\text{ZnRh}_2\text{O}_4/\text{Ag}/\text{AgSbO}_3$ (black solid circles) and $\text{ZnRh}_2\text{O}_4/\text{Ag}/\text{Ag}_{1-x}\text{Sb}_{0.3-y}$ (blue solid circles) using LED light sources (Table S1). Note that the AQE values for H_2 evolution were nearly identical as those for O_2 evolution. UV-vis spectra of as-prepared AgSbO_3 , $\text{NH}_4\text{OH} + \text{H}_2\text{O}_2$ -treated AgSbO_3 , and HNO_3 -treated AgSbO_3 are also shown. The AQE values by $\text{ZnRh}_2\text{O}_4/\text{Ag}/\text{Ag}_{1-x}\text{Sb}_{0.3-y}$ were obtained from a previous report [22]. (For interpretation of the references to colour in this figure legend, the reader is referred to the web version of this article.)

was extended to 660 nm and the photocatalytic activity was also greatly enhanced.

4. Conclusions

We established a visible-light-sensitive solid-state Z-scheme photocatalyst for overall pure-water splitting by inserting Ag between ZnRh_2O_4 and AgSbO_3 . This synthesis approach was developed based on the results of our previous study [22], which suggested that HNO_3 treatment to remove excess Ag produced the defective AgSbO_3 ($\text{Ag}_{1-x}\text{Sb}_{0.3-y}$), leading to a narrowed range of wavelength sensitivity and decreased photocatalytic water-splitting activity. To avoid these adverse effects, we utilized $\text{NH}_4\text{OH} + \text{H}_2\text{O}_2$ treatment to generate $\text{ZnRh}_2\text{O}_4/\text{Ag}/\text{AgSbO}_3$, which was sensitive to wavelengths up to 660 nm and had markedly enhanced water-splitting activity. In addition to the production of H_2 by the photocatalytic water-splitting reaction, the utilization of carbon dioxide for the production of fuels and valuable chemi-

cals has attracted growing attention. $\text{ZnRh}_2\text{O}_4/\text{Ag}/\text{AgSbO}_3$ has the potential to reduce carbon dioxide to carbon monoxide, formate, methanol, methane, and other hydrocarbons using water as an electron source under visible-light illumination. Such studies are currently underway in our laboratory.

Acknowledgements

This study was supported by the Cooperative Research Program of Institute for Catalysis, Hokkaido University (Grant #16A1002) and partially by JKA with promotion funds from KEIRIN RACE (Grant #28-146). We express gratitude to Mr. G. Newton for the careful reading of the manuscript.

Appendix A. Supplementary data

Supplementary data associated with this article can be found, in the online version, at <http://dx.doi.org/10.1016/j.apcatb.2017.03.040>.

References

- [1] A. Fujishima, K. Honda, *Nature* 238 (1972) 37–38.
- [2] J. Sato, N. Saito, H. Nishiyama, Y. Inoue, *J. Phys. Chem. B* 105 (2001) 6061–6063.
- [3] H. Kato, K. Asakusa, A. Kudo, *J. Am. Chem. Soc.* 125 (2003) 3082–3089.
- [4] K. Maeda, K. Teramura, D. Lu, T. Takata, N. Saito, Y. Inoue, K. Domen, *Nature* 440 (2006) 295.
- [5] Y. Lee, H. Terashima, Y. Shimodaira, K. Teramura, M. Hara, H. Kobayashi, K. Domen, M. Yashima, *J. Phys. Chem. C* 111 (2007) 1042–1048.
- [6] H. Liu, J. Yuan, W. Shangguan, Y. Teraoka, *J. Phys. Chem. C* 112 (2008) 8521–8523.
- [7] N. Lei, M. Tanabe, H. Irie, *Chem. Commun.* 49 (2013) 10094–10096.
- [8] L. Liao, Q. Zhang, Z. Su, Z. Zhao, Y. Wang, Y. Li, X. Lu, D. Wei, G. Feng, Q. Yu, X. Cai, J. Zhao, Z. Ren, H. Fang, F.R. Hernández, S. Baldelli, J. Bao, *Nat. Nanotechnol.* 9 (2014) 69–73.
- [9] C. Pan, T. Takata, M. Nakabayashi, T. Matsumoto, N. Shibata, Y. Ikuhara, K. Domen, *Angew. Chem. Int. Ed.* 54 (2015) 2955–2960.
- [10] J. Liu, Y. Liu, N. Liu, Y. Han, X. Zhang, H. Huang, Y. Lifshitz, S.T. Lee, J. Zhong, Z. Kang, *Science* 347 (2015) 970–974.
- [11] H. Kato, A. Kudo, *J. Phys. Chem. B* 105 (2001) 4285–4292.
- [12] H. Kato, K. Kobayashi, A. Kudo, *J. Phys. Chem. B* 106 (2002) 12441–12447.
- [13] H. Kato, A. Kudo, *J. Phys. Chem. B* 106 (2002) 5029–5034.

- [14] K. Sayama, A. Nomura, T. Arai, T. Sugita, R. Abe, M. Yanagida, T. Oi, I. Iwasaki, Y. Abe, H. Sugihara, *J. Phys. Chem. B* 110 (2006) 11352–11360.
- [15] W. Yao, J. Ye, *J. Phys. Chem. B* 110 (2006) 11188–11195.
- [16] R. Konta, T. Ishii, H. Kato, A. Kudo, *J. Phys. Chem. B* 108 (2004) 8992–8995.
- [17] K. Sayama, K. Mukasa, R. Abe, Y. Abe, H. Arakawa, *J. Photochem. Photobiol. A*: *Chem.* 148 (2002) 71–77.
- [18] H. Kato, Y. Sasaki, A. Iwase, A. Kudo, *Bull. Chem. Soc. Jpn.* 80 (2007) 2457–2464.
- [19] A. Kudo, *Int. J. Hydrogen Energy* 32 (2002) 2673–2678.
- [20] Y. Sasaki, H. Nemoto, K. Saito, A. Kudo, *J. Phys. Chem. C* 113 (2009) 17536–17542.
- [21] A. Iwase, Y.H. Ng, Y. Ishiguro, A. Kudo, R. Amal, *J. Am. Chem. Soc.* 133 (2011) 11054–11057.
- [22] R. Kobayashi, S. Tanigawa, T. Takashima, B. Ohtani, H. Irie, *J. Phys. Chem. C* 118 (2014) 22450–22456.
- [23] R. Kobayashi, K. Kurihara, T. Takashima, B. Ohtani, H. Irie, *J. Mater. Chem. A* 4 (2016) 3061–3067.
- [24] R. Kobayashi, T. Takashima, S. Tanigawa, S. Takeuchi, B. Ohtani, H. Irie, *Phys. Chem. Chem. Phys.* 18 (2016) 27693–28378.
- [25] H. Wiggers, U. Simon, G. Schön, *Solid State Ion.* 107 (1998) 111–116.
- [26] J.P. Allen, M.K. Nilsson, D.O. Scanlon, G.W. Watson, *Phys. Rev. B* 83 (2011) 035207/1–8.
- [27] T. Kako, N. Kikugawa, J. Ye, *Catal. Today* 131 (2008) 197–202.
- [28] W. Erbs, J. Desilvestro, E. Borgarello, M. Gratzel, *J. Phys. Chem.* 88 (1984) 4001–4006.